Nano Research 2016, 9(10): 2852–2861
DOI 10.1007/s12274-016-1165-z
Research Article
ISSN 1998-0124
CN 11-5974/O4

Strategies to obtain pattern fidelity in nanowire growth from large-area surfaces patterned using nanoimprint lithography

Gaute Otnes, Magnus Heurlin, Mariusz Graczyk, Jesper Wallentin[†], Daniel Jacobsson[‡], Alexander Berg, Ivan Maximov, and Magnus T. Borgström (✉)

Solid State Physics, Lund University, Box 118, S-221 00 Lund, Sweden
[†] *Present address: Division of Synchrotron Radiation Research, Lund University, Box 118, S-221 00 Lund, Sweden*
[‡] *Present address: nCHREM/Centre for Analysis and Synthesis, Lund University, Box 124, S-221 00 Lund, Sweden*

Received: 10 May 2016
Accepted: 1 June 2016

KEYWORDS
semiconductor, nanowire, nanoimprint lithography, metal–organic vapor phase epitaxial (MOVPE), patterning

ABSTRACT

Position controlled nanowire growth is important for nanowire-based optoelectronic components which rely on light emission or light absorption. For solar energy harvesting applications, dense arrays of nanowires are needed; however, a major obstacle to obtaining dense nanowire arrays is seed particle displacement and coalescing during the annealing stage prior to nanowire growth. Here, we explore three different strategies to improve pattern preservation of large-area catalyst particle arrays defined by nanoimprint lithography for nanowire growth. First, we see that heat treating the growth substrate prior to nanoimprint lithography improves pattern preservation. Second, we explore the possibility of improving pattern preservation by fixing the seed particles in place prior to annealing by modifying the growth procedure. And third, we show that a SiN_x growth mask can fully prevent seed particle displacement. We show how these strategies allow us to greatly improve the pattern fidelity of grown InP nanowire arrays with dimensions suitable for solar cell applications, ultimately achieving 100% pattern preservation over the sampled area. The generic nature of these strategies is supported through the synthesis of GaAs and GaP nanowires.

1 Introduction

Nanowires (NWs) have been identified as one of the most promising nanoscale building blocks for the next generation of electronic and optoelectronic devices such as transistors [1], light-emitting diodes [2], and solar cells [3]. NW solar cell research is rapidly evolving [4] because efficient light trapping by these antenna-like structures has been theoretically predicted [5] and experimentally proven [6, 7]. In particular,

Address correspondence to magnus.borgstrom@ftf.lth.se

theoretical modeling based on wave optics has predicted diameter-dependent resonant light-trapping in NW arrays [8–10], which allows bulk-like photocurrent generation in NW-based solar cells with just a fraction of the material consumption in comparison with thin film solar cells of the same material [3].

To achieve high-efficiency NW-based solar cells, high quality NW growth from patterned substrates is required [4]. Substrate patterning for NW growth is most commonly achieved using electron beam lithography (EBL) [11] or nanoimprint lithography (NIL)[12]. Other techniques [13] such as nanosphere lithography [14, 15] and laser interference lithography [16] have been used to a lesser extent. While EBL is incompatible with large scale industrial implementation, NIL has the potential of large-area and high-throughput patterning. For particle-assisted growth, the seed particle can be defined in the pattern by self-catalysis [17], metal evaporation [18] or metal electroplating, which allows significant material economization [19]. Epitaxial growth sets high demands with respect to pre-preparation of the substrate surface before growth. It is thus important to better understand the effect of the NIL process on the subsequent NW growth. Furthermore, axially defined p-i-n junctions in InP NWs with a diameter and pitch designed for optimal absorption [6] have not yet been reported. From a synthetic view point, the choice of pattern used for growth will strongly affect the growth dynamics. Hence, there is a need to optimize the nucleation and growth of dense patterns defined by a large NIL patterning area.

We report the metal-seed-particle-assisted synthesis of InP NWs grown in the vapor–liquid–solid growth mode using a low-pressure metal–organic vapor phase epitaxy (MOVPE) system. The seed particles consisted of gold, and were defined in a pattern using NIL, metal evaporation, and lift-off. InP NW synthesis from a pattern with dimensions corresponding to maximum light absorption (hexagonal arrangement with a diameter of 200 nm and a pitch of 500 nm) typically resulted in seed particles moving around the surface and coalescing under standard annealing, nucleation, and growth conditions. Hence, the optimal pattern for light absorption was destroyed. Furthermore, this leads to non-uniform growth conditions, problems with reproducibility, and difficulties in subsequent vertical processing of the arrays into solar cell devices. Here we explore three strategies to prevent gold seed particles from coalescing. First, we implement a heat treatment step in the beginning of the NIL procedure, second we introduce a pre-anneal nucleation step to the growth procedure, and third we use a SiN_x growth mask between the gold particles. These strategies have allowed us to improve the preservation of the original NIL-pattern during NW growth, achieving 100% fidelity in the pattern over the sampled area.

2 Experimental details

First, we will describe what constituted our standard NIL and NW growth procedure, and then we will introduce the three modifications to the standard procedure investigated in this article.

2″ InP:Zn (111)B wafers were imprinted by NIL using an Intermediate Polymer Stamp in a Simultaneous Thermal and UV-process (IPS-STU), developed by Obducat AB [20]. Two different imprint stamps were used to define the pattern of gold particles: one giving a square pattern with a pitch of 400 nm and diameter of 150 nm and one giving a hexagonal pattern with a pitch of 500 nm and diameter of 200 nm (optimized for light absorption). All wafers were covered with a double-layer resist by two subsequent steps, consisting of spin coating and curing of first LOR 0.7A and then TU7-120. The pattern of holes was transferred from the IPS to the TU7-120 using a 6″ nanoimprinter from Obducat AB, after which descumming with O_2 reactive ion etching and undercutting with diluted Microposit MF319 developer was carried out. Then the desired thickness of gold was evaporated onto the surface, followed by lift-off using Microposit Remover 1165 to remove the double-layer resist and excess gold. After lift-off, the samples were rinsed with DI water and blown dry with N_2.

The imprinted 2″ wafers were cleaved into smaller samples which were used for the growth experiments. The growth experiments were carried out in two similar low pressure (100 mbar) MOVPE reactors using hydrogen (H_2) as the carrier gas. For the annealing temperature experiments, an Epiquip MOVPE with a total flow of 6 L/min was used while the remaining

experiments were carried out in an Aixtron 200/4 MOVPE with a total flow of 13 L/min. The samples were heated to an annealing temperature of 550 ˚C under a flow of phosphine (PH_3, χ_{PH_3}= 6.9 × 10^{-3}), and annealed for 10 min to desorb any surface oxides. After the annealing step, the chamber was cooled to the growth temperature of 440 ˚C. Then, after a 2 min temperature stabilization step, InP NW growth was initiated by introducing trimethylindium (TMIn) at a molar faction of χ_{TMIn} = 5.9 × 10^{-5} and diethylzinc (DEZn) as a p-type dopant precursor at a molar fraction of χ_{DEZn} = 9.2 × 10^{-7}. To ensure the compatibility of this procedure with NW growth for solar cell devices, a p-doped NW base was used to ensure good contact with the p-type InP substrate. After 15 s, hydrogen chloride (HCl) was introduced to the growth chamber at a molar fraction of χ_{HCl} = 4.6 × 10^{-5} in order to suppress radial growth [21]. The growth time was 24.5 min, after which the flow of TMIn and HCl was switched off, and the chamber cooled to 300 ˚C under a PH_3/H_2 mixture.

The effect of the following three modifications to the standard procedure on pattern preservation was investigated.

(1) Heat treatment before imprinting: Prior to spinning the resist, the wafers were subject to a 10 min heat treatment on a hot plate at 200 ˚C.

(2) Pre-anneal nucleation: Before annealing in the growth chamber, TMIn and DEZn at molar fractions of χ_{TMIn} = 5.9 × 10^{-5} and χ_{DEZn} = 9.2 × 10^{-7}, were added to the flow of χ_{PH_3}= 6.9 × 10^{-3} at a specified temperature. After 1 min, the TMIn and DEZn flow was stopped and the temperature was increased to an annealing temperature of 550 ˚C with χ_{PH_3} = 3.5 × 10^{-2} to prevent phosphorous desorption. Then the reactor was cooled to 440 ˚C and the growth proceeded under the same flow rates, gases, and parameters as described above for the standard growth procedure. For all experiments with pre-anneal nucleation, the heat treatment before imprinting was used.

(3) NW growth using a SiN_x growth mask: For making the growth mask, wafers had a 65–70 nm thick SiN_x layer deposited prior to NIL by plasma enhanced chemical vapor deposition (PECVD). Between the steps of undercut formation and gold evaporation under the standard imprinting procedure, holes were made in the mask by CHF_3/CF_4 reactive ion etching, after which a 10 s dip in HF:H_2O 1:100 was used to remove any residues. For growth using the SiN_x-growth mask, an annealing temperature of 625 ˚C (10 min) was used in the MOVPE chamber. During the first 180 s of NW growth, the phosphine flow was lowered to χ_{PH_3}= 1.5 × 10^{-3}. For all experiments employing a SiN_x growth mask, the heat treatment before imprinting was used.

Gold seed particle coalescence was evaluated from top-view scanning electron microscope (SEM) images of the grown NWs. The number of NWs in a certain image was extracted using the software ImageJ [22] from which the density of NWs was evaluated. Seed particle coalescence leads to decreased NW density, which in this work will be used as a measure of pattern preservation. At least four different areas of each sample were investigated, each area being 2,200 μm^2 and containing 10,230 wires on a perfect sample.

The optical properties of the grown NWs were evaluated by photoluminescence (PL) at 5 K. Single NWs were broken off of the native substrate and transferred to a gold covered silicon substrate. They were excited by a CW laser emitting at 532 nm. A liquid N_2-cooled CCD camera was used to record the resulting PL signal after it had been collected through an optical microscope and dispersed by a spectrometer.

3 Results and discussion

3.1 Heat treatment before imprinting

Figure 1 illustrates the sensitivity of the NW growth on the preparation of the substrate surface, showing NWs grown from NIL patterned substrates from three different wafers imprinted by the same stamp. In Figs. 1(a) and 1(b), growth and processing conditions are nominally identical but result in a large difference in pattern preservation. Both substrates were patterned without using a heat treatment before imprinting and NWs were grown without using a pre-anneal nucleation step (direct heating in the growth chamber to 550 ˚C for 10 min annealing, after which the sample was cooled to 440 ˚C, at which point NW growth was initiated). The pattern is destroyed at some stage of the process before the NWs nucleated. We observe

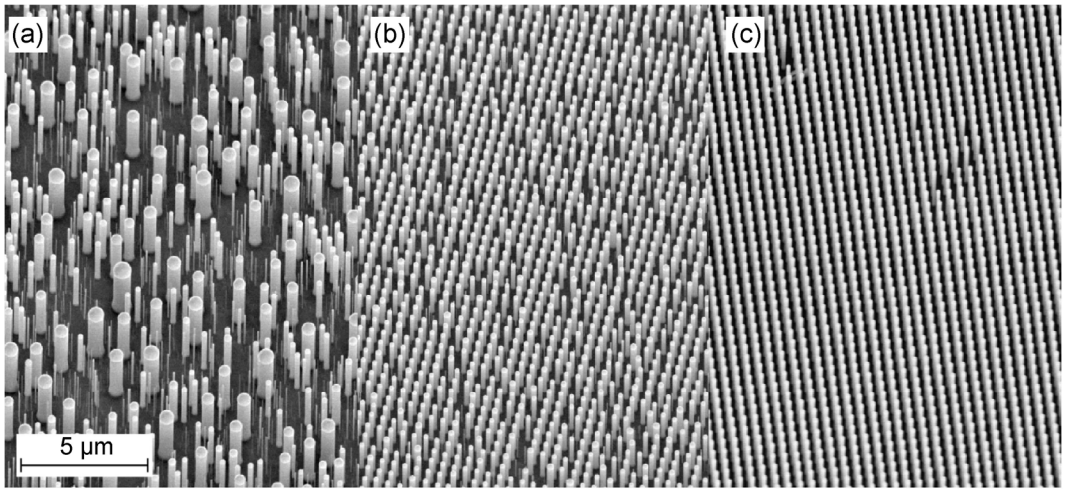

Figure 1 InP NWs grown from NIL-defined gold seed particle arrays, (a) and (b) after annealing at 550 ˚C for 10 min, cooling down to and growth at 440 ˚C, (c) after heating the substrate for 10 min at 200 ˚C before imprinting, annealing at 550 ˚C for 10 min, cooling down to and growth at 440 ˚C. Note that (a) and (b) were processed with nominally identical parameters, yet exhibit very different degrees of pattern preservation.

gold particle diameters after growth corresponding to integer multiples of the initial gold particle volume. We conclude that particle movement and coalescing is the dominant mechanism of pattern disintegration. The large difference between the two samples produced in nominally the same way (Figs. 1(a) and 1(b)) indicates that particle coalescence is very sensitive to the surface conditions, which are influenced by the process steps during the NIL pattern formation. In Fig. 1(c) a heat treatment before imprinting on a hotplate at 200 ˚C for 10 min has been used and this reduces the number of coalesced particles, resulting in improved pattern preservation. This step was initially used to remove water from the substrate surface, but we attribute its effect on pattern preservation to a thickened oxide on the InP surface during heat treatment, as indicated by X-ray photoelectron spectroscopy (XPS)-measurements (not shown here). We speculate that the thicker oxide, due to incomplete desorption during heating to annealing temperatures, can prevent lateral movement of the Au alloy particles. The surface oxide has been observed to desorb more easily in the vicinity of gold particles [23, 24], which is the most likely reason that the oxide is preserved between the particles but not underneath.

Even though heat treatment before imprinting reduces particle coalescence, the degree of pattern preservation is not satisfactory when using a high density pattern of gold particles needed for the synthesis of NW arrays in the geometry for optimal light absorption [25]. Especially we see that the pattern preservation worsens when evaporating the thicker gold films necessary to achieve the desired NW diameter (see the Electronic Supplementary Material (ESM)).

3.2 The influence of annealing temperature on gold particle movement

To reduce gold particle movement, it is useful to better understand the possible underlying mechanisms. We argue that two factors are important in governing particle movement which subsequently leads to particle coalescence. First, the particle needs to be in a liquid state, and second, it needs to be in contact with the substrate surface such that it can freely move. Let us first discuss how the particle can reach a liquid state. The Au–In binary system has a eutectic point at an In composition of 35%–40% and a temperature of about 450 ˚C [26]. For the gold particle to reach a composition at which it can melt at the annealing temperatures studied here, it needs to approach the eutectic composition by going through solid state phase transformations, studied by several authors [27–30]. Fatemi and Weizer [29] showed how the first step of this process is the dissociative diffusion of In into gold, until the solubility limit is reached. They

showed that this process is governed by the self-diffusion (vacancy diffusion) of gold, a process for which they measured an activation energy in the vicinity of 1 eV, while others have reported an activation energy of 1.8 eV [31]. When the solid state solubility is reached, the Au_3In-phase may form. This would be governed by the release of In from InP at the InP–Au interface, with an activation energy reported to be in the vicinity of 2.5 eV [29, 30].

We performed experiments where NWs were grown using various annealing temperatures, from 500 to 650 ˚C. The pattern preservation was analyzed by studying the NW density. The results are summarized in the Arrhenius plot in Fig. 2. Our data indicate that particle movement is a thermally activated process with an activation energy of 1.9 eV. It is not possible from our data to determine which of the previously mentioned solid state reactions are dominant, but we note that the value we find is in good agreement with the activation energies reported for the dissolution of In into gold to reach the eutectic composition. As soon as the particle is in a molten state, we expect the InP dissolution reactions to be enhanced due to rapid diffusion into the liquid Au–In alloy particle and more

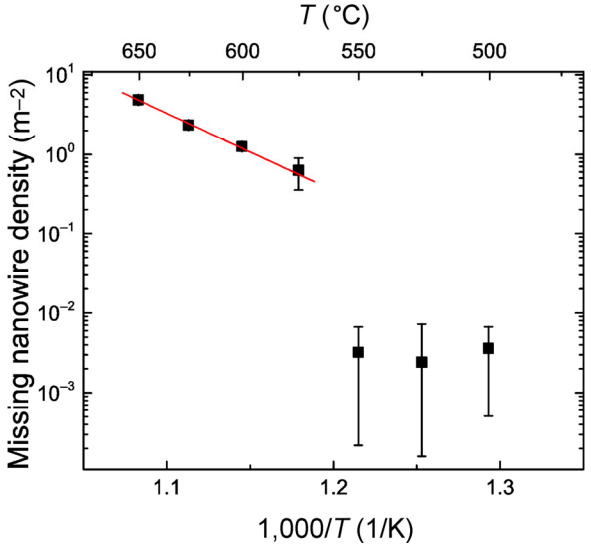

Figure 2 Arrhenius plot of NW density when annealing at different temperatures. An Arrhenius fit (red line) yields an activation energy of 1.9 eV for the process. In this experiment, annealing at the three lowest temperatures (below 575 ˚C) gave close to perfect pattern preservation, and did not show any Arrhenius behavior.

effective desorption of In and P. Establishing the driving force for the lateral movement of the Au–In liquid particle on the substrate surface is beyond the scope of this paper, but we note that liquid Ga particles have been shown to move on a GaP (111)B surface driven by the affinity of the liquid particles to cover steps and surface roughness [24], which might partly explain Au movement in this current research.

3.3 Pre-anneal nucleation

To improve pattern preservation for the highest density pattern used, we implemented an additional pre-anneal nucleation step in the growth scheme. We tried to grow a short InP NW stub before annealing to fix the gold particle in place. We investigated the effect of the pre-anneal nucleation temperature, which was varied from 280 to 420 ˚C (pre-anneal nucleation lasted for 1 min, with $\chi_{TMIn} = 5.9 \times 10^{-5}$, $\chi_{DEZn} = 9.2 \times 10^{-7}$, and $\chi_{PH_3} = 6.9 \times 10^{-3}$). Pre-anneal nucleation has a strong influence on pattern preservation. NWs grown with three different pre-anneal nucleation temperatures are shown in the top-view SEM images of Figs. 3(a)–3(c). At 320 ˚C (Fig. 3(a)), no missing NWs are observed in the pattern. The evaluation of missing NW density as a function of different pre-anneal nucleation temperatures, ranging from 280–420 ˚C, is shown in Fig. 3(d). The missing NW density decreases from 1.1 to 0.0 μm^{-2} (1.4 μm^{-2} without the use of pre-anneal nucleation) as the pre-anneal nucleation temperature decreases from 420 ˚C. The preservation is excellent for the pre-anneal nucleation temperatures equal to and below 320 ˚C. Slight shifts of the exact NW position compared to the imprinted pattern can still be observed at the lowest temperatures. However, for these samples where low-temperature pre-anneal nucleation was used, a very low density of thick NWs resulting from coalesced seed particles was observed in the investigated areas.

In order to better understand the temperature dependence of the pre-anneal nucleation step with respect to the improved quality of the NW pattern, we carried out experiments where growth was interrupted immediately after the pre-anneal nucleation step and after the annealing step, for selected pre-anneal nucleation temperatures. Here, we find it instructive to

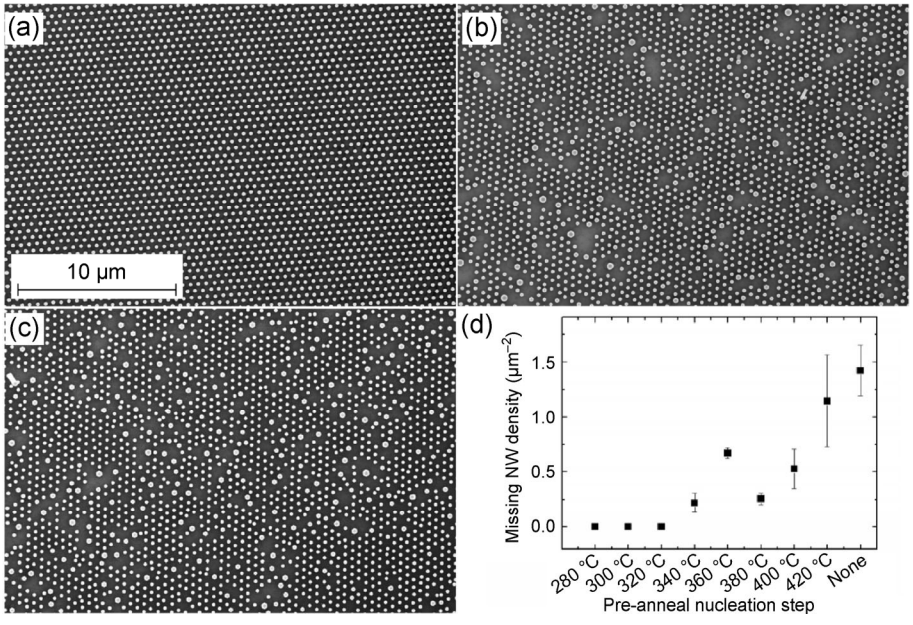

Figure 3 Top-view SEM image of NWs grown after pre-anneal nucleation (1 min, with $\chi_{TMIn} = 5.9 \times 10^{-5}$, $\chi_{DEZn} = 9.2 \times 10^{-7}$, and $\chi_{PH_3} = 6.9 \times 10^{-3}$) at (a) 320 ˚C, (b) 360 ˚C, and (c) 420 ˚C. (d) The density of missing NWs after growth is a function of different pre-anneal nucleation temperatures. "None" indicates that no pre-anneal nucleation step was included in the growth procedure.

present the two extremes, pre-anneal nucleation at 280 and 420 ˚C, with SEM images shown in Fig. 4. Results of pre-anneal nucleation at 420 ˚C followed by cooling, Fig. 4(a), show that growth has taken place from the characteristic hemispherical molten gold particle. It is interesting to note that little or no particle merging has occurred, which indicates that the movement and coalescence of particles shown in Fig. 3 occurs after the pre-anneal nucleation step. In the corresponding experiment where growth was interrupted after pre-anneal nucleation and high temperature annealing (Fig. 4(b)), the NW stub is no longer visible and particle displacement is observed. This indicates that the ~100 nm long stem grown after the pre-anneal nucleation (Fig. 4(a)) is decomposed during the annealing phase before re-initiating NW growth. We speculate that the liquid particle can move on the substrate surface after the stub is consumed. It should be noted here that fixing the particle in place by growing a stub before annealing might still be a viable approach, if the stub is sufficiently long. However, the material quality of such a stub, grown while oxides are likely still present on the substrate surface, is questionable which is why we did not pursue this approach further.

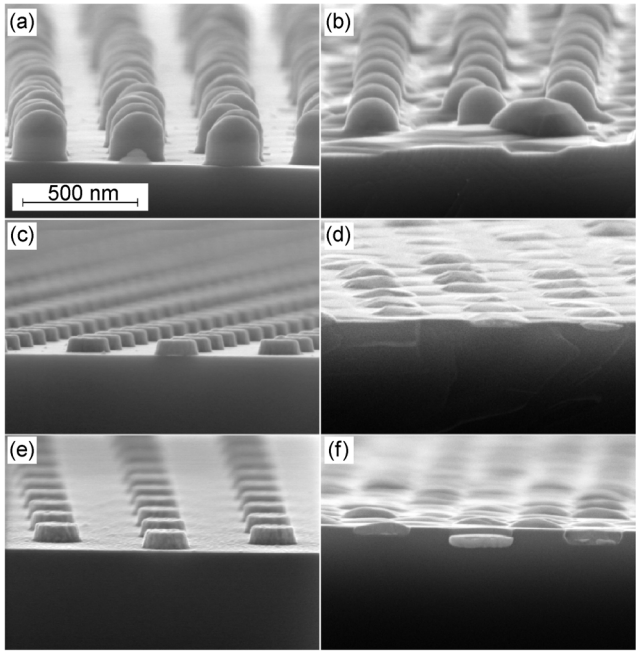

Figure 4 Cross-sectional SEM images of the sample after (a) pre-anneal nucleation at 420 ˚C, (b) pre-anneal nucleation at 420 ˚C and annealing at 550 ˚C, (c) pre-anneal nucleation at 280 ˚C, (d) pre-anneal nucleation at 280 ˚C and annealing at 550 ˚C, (e) NIL and lift-off, and (f) after annealing at 550 ˚C only. Pre-anneal nucleation lasted for 1 min, with $\chi_{TMIn} = 5.9 \times 10^{-5}$, $\chi_{DEZn} = 9.2 \times 10^{-7}$, and $\chi_{PH_3} = 6.9 \times 10^{-3}$. Annealing lasted for 10 min at 550 ˚C, with $\chi_{PH_3} = 3.5 \times 10^{-2}$.

After pre-anneal nucleation at 280 ˚C (Fig. 4(c)), the shape of the particle closely resembles that of the gold particle directly after imprinting (Fig. 4(e)), indicating that the particle is still solid, likely in the α-phase [26]. If any stem is grown, it is too small to be observed by SEM imaging and most probably grown in the vapor–solid–solid growth mode. On the other hand, after annealing, we see that the particle lies in a depression on the substrate surface (Fig. 4(d)). The particle is trapped, unable to easily slide on the surface, by the indentation made upon dissolving the InP surface underneath the gold. Interestingly, a very similar situation is found when inspecting samples that are annealed with no pre-anneal nucleation step (Fig. 4(f)). In contrast to this apparent similarity, the improvement we see in pattern preservation when introducing the pre-anneal nucleation step at low temperatures is obvious (Fig. 3). By assuming that In dissolution from the substrate is the rate limiting step, we speculate that by introducing TMIn to the growth chamber at temperatures around 300 ˚C, the excess In concentration in the gold particles, in combination with the relatively slow dissolution of the InP from the substrate, allows the alloyed gold particles to reproducibly reach the composition required to melt at a relatively low temperature, allowing a depression to form underneath the particle. Supporting this hypothesis, we see that pattern preservation worsens upon increasing the PH_3 molar fraction during annealing (see the ESM). These results indicate the strong sensitivity of NW pattern preservation on the pre-anneal nucleation conditions. Therefore, the pre-anneal nucleation must be optimized for different materials, taking into account both the substrate chemistry and the NW melting and consumption processes. In parallel with the work on InP, we performed a similar study on GaAs NWs which showed a positive effect from the pre-anneal nucleation approach using somewhat different parameters (see the ESM).

Although we see great improvement in the yield and reproducibility of pattern preservation when implementing the pre-anneal nucleation step in our growth procedure, some imperfections are still present. Most wafers show a missing NW density of <0.01 μm^{-2}, but we see that approximately 1 in 5 wafers still have a somewhat poorer pattern preservation, in the range of 0.05–0.2 μm^{-2}. We attribute the observed variability to small unintended deviations in the NIL procedure.

3.4 NW Growth with a SiN_x growth mask

As an alternative approach to obtain a high degree of pattern preservation, we also explored the possibility of adding a growth mask to the substrate surface. A growth mask of either SiN_x or SiO_x is commonly used in catalyst-free selective area NW growth [32, 33], and in self-catalyzed NW growth [34, 35]. A growth mask has been successfully used for metal-catalyzed Si microwires [36, 37] and III–V NW growth [38–40]. We used a SiN_x growth mask, and achieved 100% preservation of the pattern for grown NWs over all sampled areas (see the ESM). We attribute the effect on pattern preservation to the gold particle being locked in place by the growth mask. The use of such a growth mask has the additional benefits of preventing parasitic substrate growth, as well as facilitating use of electrodeposition of gold to reduce material consumption and make reuse of the growth substrate possible [19]. We note that using a growth mask introduces additional processing requirements, and possibly alters the growth conditions due to the strong substrate surface effects on adatom migration lengths and heterogeneous pyrolysis [41]. For many purposes, the pre-anneal nucleation procedure might therefore prove sufficient. In parallel with this work, the GaP and GaAs material systems have been studied for light emitting applications using a different imprinting stamp, where similar pattern fidelity has been achieved using a SiN_x growth mask (see the ESM).

3.5 Photoluminescence

In order to investigate the quality of the resulting NW materials as a function of pre-anneal nucleation temperature, PL characterization was performed on single InP NWs taken from samples grown after pre-anneal nucleation at 280, 320, 380, and 420 ˚C, as well as from the reference sample grown without any pre-anneal nucleation. Four to five single NWs were measured from each sample. All of the NWs

from all of the samples show multiple sharp peaks corresponding to optical transitions at energies lying between the band gap of zinc blend (ZB) (1.42 eV) and wurtzite (WZ) (1.49 eV) InP. Such optical transitions are commonly seen in InP NWs with mixed crystal structure and twin planes distributed along the length of the wire [42–45]. A mixed crystal structure was confirmed by transmission electron microscope (TEM) observation (see the ESM). Both NWs grown with a pre-anneal nucleation at 280 ˚C and without pre-anneal nucleation had similar crystal structure; a ZB crystal structure with twin planes at the base, which transitioned into a WZ crystal structure with stacking faults towards the top of the nanowire. A sum of all single NW spectra taken from each sample is shown in Fig. 5. All samples show similar luminescence behavior. A small exception is the sample where pre-anneal nucleation was performed at 320 ˚C, where the luminescence spectrum is smoother and less evenly distributed between the band gaps of the two crystal phases. Overall, however, there is no clear change in the optical properties as a function of the pre-anneal nucleation conditions. Although not part of the current investigation, we note that the use of a SiN_x-growth mask may possibly change the optical properties since material diffusion on the substrate will be affected. This can lead to shifts in the crystal structure, as previously observed [19].

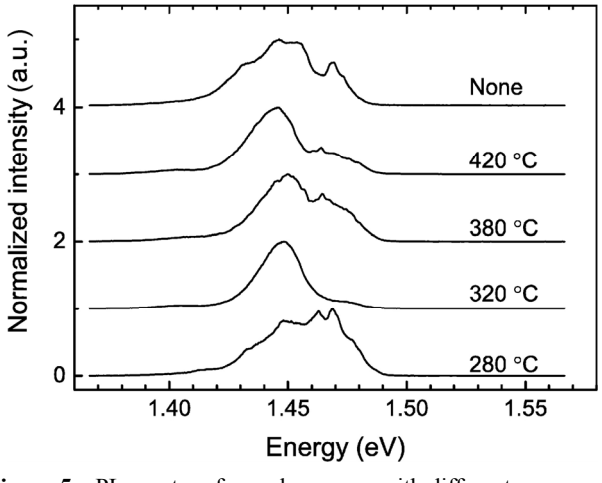

Figure 5 PL spectra of samples grown with different pre-anneal nucleation conditions. Each of the spectra shown is the sum of the spectra from 4–5 single NWs. NWs were measured at 5 K, with an excitation wavelength of 532 nm (2.33 eV).

4 Conclusions

In summary, we have presented strategies to improve pattern preservation from NIL-defined seed particle arrays to grown NWs. This is especially important for high density patterns required for energy harvesting applications. The implementation of a heat treatment step before imprinting was observed to reduce the number of coalesced particles. In order to gain better control over synthesis, the possibility to deny the particle access to move freely on the substrate surface by introducing a pre-anneal nucleation step in the growth procedure was explored. By alloying the gold particle with In at low temperatures, pattern retention was significantly improved throughout the NW growth process. We argue that loading the gold particles with In decreases the effective melting temperature of the catalytic Au alloy particle, allowing the formation of depressions in the substrate surface. These depressions prevent the thermally activated movement of the Au alloy particle. We conclude that a careful balance between the processes leading to alloy particle melting and substrate dissolution is necessary for good pattern preservation. Implementing a heat treatment before imprint and pre-anneal nucleation into our imprint and growth procedures, respectively, allowed us to greatly improve the pattern preservation in our NW arrays grown from dense patterns of gold particles defined by NIL, both in terms of absolute yield and reproducibility between wafers. However, some imperfections and variability were still present. As an alternative approach to fully preserve the quality of the original pattern, a SiN_x-growth mask was added to the substrate surface to keep the particles stationary. This has allowed us to achieve 100% pattern preservation of InP NWs in high density arrays over all sampled areas. No effect on the optical properties in the NWs was observed with respect to the different pre-anneal nucleation conditions.

We believe that these approaches, with proper adjustments to the specific material system, are generally applicable to improve the pattern preservation of imprinted seed particles to grown NW arrays, supported by the results from GaAs and GaP nanowire synthesis.

Acknowledgements

This work was performed within NanoLund and supported by the Swedish Research Council (Vetenskapsrådet), the Swedish Foundation for Strategic Research (SSF), the Knut and Alice Wallenberg Foundation, and the Swedish Energy Agency. This project has received funding from the European Union's Horizon 2020 research and innovation programme (No. 641023) (Nano-Tandem) and the European Union's Seventh Framework Programme (No. NMP3-SL-2012-280773) (NWs4Light). This publication reflects only the author's views and the funding agency is not responsible for any use that may be made of the information it contains. I. M. is thankful for the financial support from NanoLund to develop the NIL technology. The authors thank Nicklas Nilsson for the technical help with nanoimprint, and Johnas Eklöf and Alexei Zakharov (MAX-IV laboratory, Lund) for input on oxide formation by use of XPS.

Electronic Supplementary Material: Supplementary material (supporting SEM and TEM images, with experimental details) is available in the online version of this article at 10.1007/s12274-016-1165-z.

References

[1] Tomioka, K.; Yoshimura, M.; Fukui, T. A III-V nanowire channel on silicon for high-performance vertical transistors. *Nature* **2012**, *488*, 189–192.

[2] Gudiksen, M. S.; Lauhon, L. J.; Wang, J. F.; Smith, D. C.; Lieber, C. M. Growth of nanowire superlattice structures for nanoscale photonics and electronics. *Nature* **2002**, *415*, 617–620.

[3] Wallentin, J.; Anttu, N.; Asoli, D.; Huffman, M.; Åberg, I.; Magnusson, M. H.; Siefer, G.; Fuss-Kailuweit, P.; Dimroth, F.; Witzigmann, B. et al. InP nanowire array solar cells achieving 13.8% efficiency by exceeding the ray optics limit. *Science* **2013**, *339*, 1057–1060.

[4] LaPierre, R. R.; Chia, A. C. E.; Gibson, S. J.; Haapamaki, C. M.; Boulanger, J.; Yee, R.; Kuyanov, P.; Zhang, J.; Tajik, N.; Jewell, N. et al. III-V nanowire photovoltaics: Review of design for high efficiency. *Phys. Status Solidi-RRL* **2013**, *7*, 815–830.

[5] Polman, A.; Atwater, H. A. Photonic design principles for ultrahigh-efficiency photovoltaics. *Nat. Mater.* **2012**, *11*, 174–177.

[6] Anttu, N.; Abrand, A.; Asoli, D.; Heurlin, M.; Åberg, I.; Samuelson, L.; Borgström, M. Absorption of light in InP nanowire arrays. *Nano Res.* **2014**, *7*, 816–823.

[7] Chen, M. Y.; Nakai, E.; Tomioka, K.; Fukui, T. Application of free-standing InP nanowire arrays and their optical properties for resource-saving solar cells. *Appl. Phys. Express* **2015**, *8*, 012301.

[8] Hu, L.; Chen, G. Analysis of optical absorption in silicon nanowire arrays for photovoltaic applications. *Nano Lett.* **2007**, *7*, 3249–3252.

[9] Kupec, J.; Stoop, R. L.; Witzigmann, B. Light absorption and emission in nanowire array solar cells. *Opt. Express* **2010**, *18*, 27589–27605.

[10] Anttu, N.; Xu, H. Q. Coupling of light into nanowire arrays and subsequent absorption. *J. Nanosci. Nanotechno.* **2010**, *10*, 7183–7187.

[11] Mårtensson, T.; Borgström, M.; Seifert, W.; Ohlsson, B. J.; Samuelson, L. Fabrication of individually seeded nanowire arrays by vapour–liquid–solid growth. *Nanotechnology* **2003**, *14*, 1255–1258.

[12] Mårtensson, T.; Carlberg, P.; Borgström, M.; Montelius, L.; Seifert, W.; Samuelson, L. Nanowire arrays defined by nanoimprint lithography. *Nano Lett.* **2004**, *4*, 699–702.

[13] Fan, H. J.; Werner, P.; Zacharias, M. Semiconductor nanowires: From self-organization to patterned growth. *Small* **2006**, *2*, 700–717.

[14] Fuhrmann, B.; Leipner, H. S.; Höche, H.-R.; Schubert, L.; Werner, P.; Gösele, U. Ordered arrays of silicon nanowires produced by nanosphere lithography and molecular beam epitaxy. *Nano Lett.* **2005**, *5*, 2524–2527.

[15] Madaria, A. R.; Yao, M. Q.; Chi, C. Y.; Huang, N. F.; Lin, C. X.; Li, R. J.; Povinelli, M. L.; Dapkus, P. D.; Zhou, C. W. Toward optimized light utilization in nanowire arrays using scalable nanosphere lithography and selected area growth. *Nano Lett.* **2012**, *12*, 2839–2845.

[16] Kauppinen, C.; Haggren, T.; Kravchenko, A.; Jiang, H.; Huhtio, T.; Kauppinen, E.; Dhaka, V.; Suihkonen, S.; Kaivola, M.; Lipsanen, H. et al. A technique for large-area position-controlled growth of GaAs nanowire arrays. *Nanotechnology* **2016**, *27*, 1356011.

[17] Munshi, A. M.; Dheeraj, D. L.; Fauske, V. T.; Kim, D. C.; Huh, J.; Reinertsen, J. F.; Ahtapodov, L.; Lee, K. D.; Heidari, B.; van Helvoort, A. T. J. et al. Position-controlled uniform GaAs nanowires on silicon using nanoimprint lithography. *Nano Lett.* **2014**, *14*, 960–966.

[18] Pierret, A.; Hocevar, M.; Diedenhofen, S. L.; Algra, R. E.; Vlieg, E.; Timmering, E. C.; Verschuuren, M. A.; Immink, G. W. G.; Verheijen, M. A.; Bakkers, E. P. A. M. Generic nano-imprint process for fabrication of nanowire arrays. *Nanotechnology* **2010**, 065305.

[19] Jam, R. J.; Heurlin, M.; Jain, V.; Kvennefors, A.; Graczyk, M.; Maximov, I.; Borgström, M. T.; Pettersson, H.; Samuelson, L. III-V nanowire synthesis by use of electrodeposited gold particles. *Nano Lett.* **2015**, *15*, 134–138.

[20] Eriksson, T.; Yamada, S.; Krishnan, P. V.; Ramasamy, S.; Heidari, B. High volume nanoimprint lithography on III/V substrates: Imprint fidelity and stamp lifetime. *Microelectron. Eng.* **2011**, *88*, 293–299.

[21] Borgström, M. T.; Wallentin, J.; Trägårdh, J.; Ramvall, P.; Ek, M.; Wallenberg, L. R.; Samuelson, L.; Deppert, K. *In situ* etching for total control over axial and radial nanowire growth. *Nano Res.* **2010**, *3*, 264–270.

[22] Schneider, C. A.; Rasband, W. S.; Eliceiri, K. W. NIH image to ImageJ: 25 years of image analysis. *Nat. Methods* **2012**, *9*, 671–675.

[23] Hilner, E.; Lundgren, E.; Mikkelsen, A. Surface structure and morphology of InAs(111)B with/without gold nanoparticles annealed under arsenic or atomic hydrogen flux. *Surf. Sci.* **2010**, *604*, 354–360.

[24] Zakharov, A. A.; Mårsell, E.; Hilner, E.; Timm, R.; Andersen, J. N.; Lundgren, E.; Mikkelsen, A. Manipulating the dynamics of self-propelled gallium droplets by gold nanoparticles and nanoscale surface morphology. *ACS Nano* **2015**, *9*, 5422–5431.

[25] Anttu, N.; Xu, H. Q. Efficient light management in vertical nanowire arrays for photovoltaics. *Opt. Express* **2013**, *21*, A558–A575.

[26] Liu, H. S.; Cui, Y.; Ishida, K.; Jin, Z. P. Thermodynamic reassessment of the Au–In binary system. *Calphad* **2003**, *27*, 27–37.

[27] Piotrowska, A.; Auvray, P.; Guivarc'h, A.; Pelous, G.; Henoc, P. On the formation of binary compounds in Au/InP system. *J. Appl. Phys.* **1981**, *52*, 5112–5117.

[28] Weizer, V. G.; Fatemi, N. S. Contact spreading and the Au_3In-to-Au_9In_4 transition in the Au-InP system. *J. Appl. Phys.* **1990**, *68*, 2275–2284.

[29] Fatemi, N. S.; Weizer, V. G. The kinetics of the Au-InP interaction. *J. Appl. Phys.* **1990**, *67*, 1934–1939.

[30] Wada, O. Thermal reaction of gold metallization on InP. *J. Appl. Phys.* **1985**, *57*, 1901–1909.

[31] Borg, R. J.; Dienes, G. J. *An Introduction to Solid State Diffusion*; Academic Press, Inc.: San Diego, CA, 1988.

[32] Tomioka, K.; Tanaka, T.; Hara, S.; Hiruma, K.; Fukui, T. III–V nanowires on Si substrate: Selective-area growth and device applications. *IEEE J. Sel. Top. Quant.* **2011**, *17*, 1112–1129.

[33] Yao, M. Q.; Huang, N. F.; Cong, S.; Chi, C.-Y.; Seyedi, M. A.; Lin, Y.-T.; Cao, Y.; Povinelli, M. L.; Dapkus, P. D.; Zhou, C. W. GaAs nanowire array solar cells with axial p–i–n junctions. *Nano Lett.* **2014**, *14*, 3293–3303.

[34] Zhang, Y. Y.; Wu, J.; Aagesen, M.; Holm, J.; Hatch, S.; Tang, M. C.; Huo, S. G.; Liu, H. Y. Self-catalyzed ternary core–shell GaAsP nanowire arrays grown on patterned Si substrates by molecular beam epitaxy. *Nano Lett.* **2014**, *14*, 4542–4547.

[35] Russo-Averchi, E.; Vukajlovic Plestina, J.; Tütüncüoglu, G.; Matteini, F.; Dalmau-Mallorquí, A.; de la Mata, M.; Rüffer, D.; Potts, H. A.; Arbiol, J.; Conesa-Boj, S. et al. High yield of GaAs nanowire arrays on Si mediated by the pinning and contact angle of Ga. *Nano Lett.* **2015**, *15*, 2869–2874.

[36] Spurgeon, J. M.; Plass, K. E.; Kayes, B. M.; Brunschwig, B. S.; Atwater, H. A.; Lewis, N. S. Repeated epitaxial growth and transfer of arrays of patterned, vertically aligned, crystalline Si wires from a single Si(111) substrate. *Appl. Phys. Lett.* **2008**, *93*, 032112.

[37] Kendrick, C. E.; Redwing, J. M. The effect of pattern density and wire diameter on the growth rate of micron diameter silicon wires. *J. Cryst. Growth* **2011**, *337*, 1–6.

[38] Nowzari, A.; Heurlin, M.; Jain, V.; Storm, K.; Hosseinnia, A.; Anttu, N.; Borgström, M. T.; Pettersson, H.; Samuelson, L. A comparative study of absorption in vertically and laterally oriented InP core–shell nanowire photovoltaic devices. *Nano Lett.* **2015**, *15*, 1809–1814.

[39] Berg, A.; Lenrick, F.; Vainorius, N.; Beech, J. P.; Wallenberg, L. R.; Borgström, M. T. Growth parameter design for homogeneous material composition in ternary $Ga_xIn_{1-x}P$ nanowires. *Nanotechnology* **2015**, *26*, 435601.

[40] Dalacu, D.; Kam, A.; Austing, D. G.; Wu, X. H.; Lapointe, J.; Aers, G. C.; Poole, P. J. Selective-area vapour–liquid–solid growth of InP nanowires. *Nanotechnology* **2009**, *20*, 395602.

[41] Stringfellow, G. B. *Organometallic Vapor-Phase Epitaxy: Theory and Practice*, 2nd ed.; Academic Press: San Diego, CA, 1999.

[42] Mishra, A.; Titova, L. V.; Hoang, T. B.; Jackson, H. E.; Smith, L. M.; Yarrison-Rice, J. M.; Kim, Y.; Joyce, H. J.; Gao, Q.; Tan, H. H. et al. Polarization and temperature dependence of photoluminescence from zincblende and wurtzite InP nanowires. *Appl. Phys. Lett.* **2007**, *91*, 263104.

[43] Pemasiri, K.; Montazeri, M.; Gass, R.; Smith, L. M.; Jackson, H. E.; Yarrison-Rice, J.; Paiman, S.; Gao, Q.; Tan, H. H.; Jagadish, C. et al. Carrier dynamics and quantum confinement in type II ZB-WZ InP nanowire homostructures. *Nano Lett.* **2009**, *9*, 648–654.

[44] Bao, J. M.; Bell, D. C.; Capasso, F.; Erdman, N.; Wei, D. G.; Fröberg, L.; Mårtensson, T.; Samuelson, L. Nanowire-induced Wurtzite InAs thin film on zinc-blende InAs substrate. *Adv. Mater.* **2009**, *21*, 3654–3658.

[45] Mattila, M.; Hakkarainen, T.; Mulot, M.; Lipsanen, H. Crystal-structure-dependent photoluminescence from InP nanowires. *Nanotechnology* **2006**, *17*, 1580–1583.